Viscoelastic behaviour of rapid and slow self-healing hydrogels formed by densely branched arabinoxylans from *Plantago ovata* seed mucilage

Long Yu[1,2], Jason R. Stokes[1], Gleb E. Yakubov[1,3]*

1. School of Chemical Engineering, University of Queensland, Brisbane QLD 4076, Australia

2. Adelaide Glycomics, University of Adelaide, Waite Campus, Urrbrae, SA 5064, Australia.

3. School of Biosciences, University of Nottingham, Sutton Bonington Campus, LE12 5RD, United Kingdom

* Gleb.Yakubov (at) Nottingham.ac.uk

Abstract

The self-healing behaviour of materials and hydrogels in response to damage is often made possible by hydrogen bonding between polymer chains that associate to form a gel network. The dissociation rate of hydrogen bonds is expected to influence self-healing rate, gelation kinetics and hydrogel rheology. Hydrogels are formed here using highly substituted brush-like arabinoxylan obtained from *Plantago ovata* seed mucilage. Two rheologically distinct arabinoxlyans are chosen to have similar molecular weight and linkage compositions in order to enable forming gels with a similar network. The rheology of these hydrogels is characterised using small and large-amplitude oscillatory shear. The sol-gel transition is probed as a function of concentration and temperature. The temperature dependence of storage modulus is used to obtain an activation energy for hydrogen bond dissociation via the Arrhenius equation. Differences in rheology and gelation of the two arabinoxlyan hydrogels are found to be associated with a greater proportion of 'slow' and 'fast' dissociating hydrogen bonds between the polymer side-chains. In addition, this is supported by the observed rate of recovery in the storage modulus of pre-sheared gels being predicted by two relaxation modes. We also find that the enhanced presence of fast dissociations (*i.e.* weak hydrogen bonds) corresponds to gels that are more viscous and rapidly self-healing.

Keywords

Arabinoxylan; Mucilage; *Plantago ovata*; Rheology; Hydrogen bonding; Self-healing gels; SAOS; LAOS.

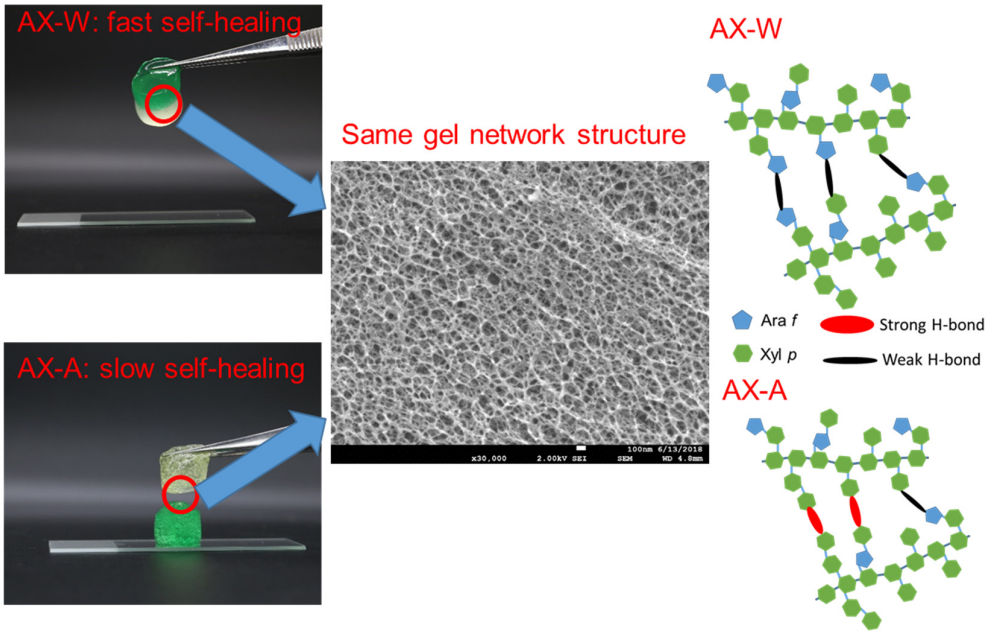

1. Introduction

Hydrogels are widely utilized in drug delivery (Hoare and Kohane 2008), food engineering (Shewan and Stokes 2013), tissue engineering (Lee and Mooney 2001), soft robotics (Zheng *et al.* 2015) and biosensors (Richter *et al.* 2008). The sub-category of self-healing hydrogels, which are able to recover their mechanical properties in response to damage, have been proposed to address such problems as limited material lifetime and improved product durability and safety (Blaiszik *et al.* 2010). Through rational design, new classes of soft materials for healthcare, food science and manufacturing industry can be developed with programmable mechanical and self-healing properties. The key challenge is to identify new routes for designing self-healing hydrogels with desired rheological properties and tuneable rates of gel re-formation (healing) properties.

Nature offers a broad range of examples of hydrogel systems, where the damaged hydrogel network recovers via reversible molecular interactions. These reversible molecular interactions mainly depend on dynamic covalent bonds and/or physical non-covalent bonds (Guimard *et al.* 2012). The reformation of dynamic covalent bonds usually requires the application of external stimulus, which makes it difficult to achieve autonomous self-healing behaviour (Taylor and in het Panhuis 2016). For that reason, the physical non-covalent bonds are generally utilized to design autonomous self-healing hydrogels. Hydrogen bonding is one of the most common mechanisms used in bulk self-healing material and ubiquitous in living system (Taylor and in het Panhuis 2016). For example, the self-complementary quadruple hydrogen-bonding functionality of ureidopyrimidinone (Upy) unit has been utilised in the development of self-healing physical hydrogels. The hydrogels undergo rapid self-healing process due to the formation of multivalent hydrogen bonding (both H-O hydrogen bonds and H-N hydrogen bonds) that is generated by the modified Upy units (Cui and del Campo 2012). Still, it remains challenging to control hydrogen bond dynamics to enable influencing the hydrogels mechanical properties and the rate of the self-healing process.

Arabinoxylans (AX) from *Plantago ovata* seed mucilage offer a unique set of structural features that enable probing the impact of hydrogen bonds dynamics on the resulting mechanical properties of hydrogels (Yu *et al.* 2018). These structural features include: a) dense side-chain decoration of the backbone (> 95 % of 1,4-linked xylose backbone sugar residues have a side-chain substitution), which reduces the impact of spatial heterogeneity of 'naked' and 'brush-like' domains on the intermolecular interactions; b) absence of charged sugar residues that can dominate inter-molecular interactions and mask the effect of hydrogen

bonding. Based on the analysis of multiscale assembly of AXs under gelled and non-gelled condition reported previously (Fischer *et al.* 2004, Guo *et al.* 2008, Yu *et al.* 2019, Yu, Yakubov, Martínez-Sanz, Gilbert and Stokes 2018, Yu *et al.* 2017), it was hypothesised that the gel formation and mechanic properties of AX hydrogels depend on small variations in the distribution of the side-chains, which are dominated by 1,3-linked arabinose and 1,3-linked xylose residues. In particular, two AX fractions from *P.ovata* seed mucilage were purified by water and alkaline solution extraction. These two polymers are shown to have very similar polymer structure and the architecture of the hydrogel network, whilst their gel properties are markedly distinct (Yu, Yakubov, Gilbert, Sewell, van de Meene and Stokes 2019, Yu, Yakubov, Zeng, Xing, Stenson, Bulone and Stokes 2017).

Here, we aim to use these AX gels to investigate the effect of hydrogen bonds on the linear and non-linear viscoelastic properties as well as autonomous self-healing behaviour. Our approach is to characterise the strength of the hydrogen bonds associated with AX chain interactions using the Arrhenius' law and gelation theory under small amplitude oscillatory shear. Further, the evolution of destruction and reformation of gel network is investigated through large amplitude oscillatory shear rheology and cyclic strain-recovery test. Finally, the autonomous self-healing behaviour of different AX gels is demonstrated by dynamic interfacial fusion of AX hydrogel blocks.

2. Materials and methods

2.1 Materials

P. ovata seeds were provided by Professor Rachel Burton and Associate Professor Matthew Tucker (University of Adelaide, Australia). All water used in experiments was reverse osmosis treated water (DI water) with resistivity of 18.2 MΩcm (Satorius Stedim).

2.2 Preparation of gel forming arabinoxylans for P. ovata seed mucilage

The mucilage fractions were prepared by stepwise extraction based on our previous work (Yu, Yakubov, Zeng, Xing, Stenson, Bulone and Stokes 2017). Briefly, *P. ovata* seeds were dispersed in 800 mL of DI water at 25 °C for 4 h under constant stirring. The suspension was then centrifuged at 10,000 g for 30 min. The remaining solid phase was dispersed in 400 mL of DI water at 65 °C for 4 h under constant stirring. The suspension was then centrifuged at 10,000 g for 30 min. The resulting solution was cooled to 4 °C to obtain a gel phase by centrifugation. The gel phase was then washed twice with DI water at 25 °C, and dispersed in

DI water, dialysed against DI water to obtain the hot water extracted fraction (AX-W fraction), which was subsequently freeze-dried for further use. The remaining solid phase was dissolved in a 0.2 M KOH solution with 0.01 mg/mL $NaBH_4$ at 25 °C for 4 h, and the solution and residues were separated by centrifugation. The alkaline extract was dialysed at room temperature for 48 h against DI water to obtain the so-called AX-A fraction, which was subsequently freeze-dried for further use.

2.3 Rheological characterisation: small amplitude oscillatory shear (SAOS) and large amplitude oscillatory shear (LAOS)

A series of samples ranging from 1 to 50 mg/mL in H_2O were prepared by dissolving the freeze-dried materials in DI water at 65°C for 6 h, and kept for next 3h at 85°C. The rheological tests were performed on AR G2 rheometer (TA Instruments, USA) at 25°C with a Peltier temperature control unit on bottom plate. After loading the sample, the edge of geometry was carefully trimmed and filled with low viscosity silicone oil to prevent the possible water evaporation. The samples were left to rest for 5 min before each measurement. The parallel plate with 40 mm diameter and 0.5 mm of gap were used in all the tests.

In the steady shear test, the measurements were performed at shear stress from 0.05 to 50 Pa. For the oscillatory shear tests, the strain sweep from 1% to 1,000% were completed at 6.28 rad/s to determine the linear and non-linear viscoelastic region. As for the SAOS that was tested in linear viscoelastic region (strain γ <10%), the frequency sweep in the range from 62.8 to 0.0628 rad/s were performed at varied temperature in the range from 25 °C to 65°C and pH in the range from 3 to 12. Moreover, in order to estimate the energy of hydrogen bonding in AX hydrogels, the temperature sweep from 25 to 85°C was conducted at 6.28 rad/s frequency and 5% strain. The LAOS experiments were performed at 25 °C and 6.28 rad/s, and initial stain sweep was set from 10% to 1,000%. The raw data of responsive strain, strain rate and stress were used to plot the Lissajous curves.

2.4 Self-healing properties of arabinoxylans from P. ovata seed mucilage

Dynamic strain amplitude cyclic test was conducted at a fixed angular frequency (6.28 rad/s) and 25°C. The AX hydrogels (5% w/v) were prepared and placed on AR G2 rheometer as described in section 2.3. The parallel plates with 40 mm diameter and 0.5 mm of gap were used in all the tests. Amplitude oscillatory strains were switched from small strain (γ = 5.0%) to large strain (γ = 500% or 1,000%) with 300 s for every strain interval.

To evaluate the self-healing rate of hydrogels, two hydrogel blocks of 5% (w/v) were prepared separately. After that, the hydrogel blocks were put together. The upper gel cylinder was lifted by tweezer immediately (<10 s) or after 4h to illustrate the degree of fusion between two hydrogel blocks.

3. Results and discussions

3.1 Sol-gel transition in the linear viscoelastic region

Here we explore the concentration dependent linear viscoelastic properties of the AX-A (alkaline extracted fraction) and AX-W (hot water extracted fraction) solutions in water to determine the sol-gel transition. Figure 1 shows the dependency of *G'* and loss modulus (*G"*) as a function of polysaccharide concentration at a frequency of 6.28 rad/s. At concentrations below 3 mg/mL, both polymer solutions behave as viscoelastic fluids (*G" > G'*). With increasing concentration from 1 to 3 mg/mL, we observe the progressive increase of the G'. Between 3 and 4 mg/mL, we observe a transition from the viscous (*G" > G'*) to elasticity-dominated viscoelastic behaviour (*G' > G"*). For concentrations above 4 mg/mL, our previous small angle X-ray and neutron scattering analysis indicated that such concentrated solutions have a gel-like network structure (Yu, Yakubov, Gilbert, Sewell, van de Meene and Stokes 2019, Yu, Yakubov, Martínez-Sanz, Gilbert and Stokes 2018, Yu, Yakubov, Zeng, Xing, Stenson, Bulone and Stokes 2017). These insights combined with rheological characterisation showing a weak-frequency dependence of the moduli characteristic of a gel (Yu, Yakubov, Gilbert, Sewell, van de Meene and Stokes 2019, Yu, Yakubov, Martínez-Sanz, Gilbert and Stokes 2018, Yu, Yakubov, Zeng, Xing, Stenson, Bulone and Stokes 2017) enable us to define the sol-gel transition as a point where G' = G'' at a frequency of 6.28 rad/s.

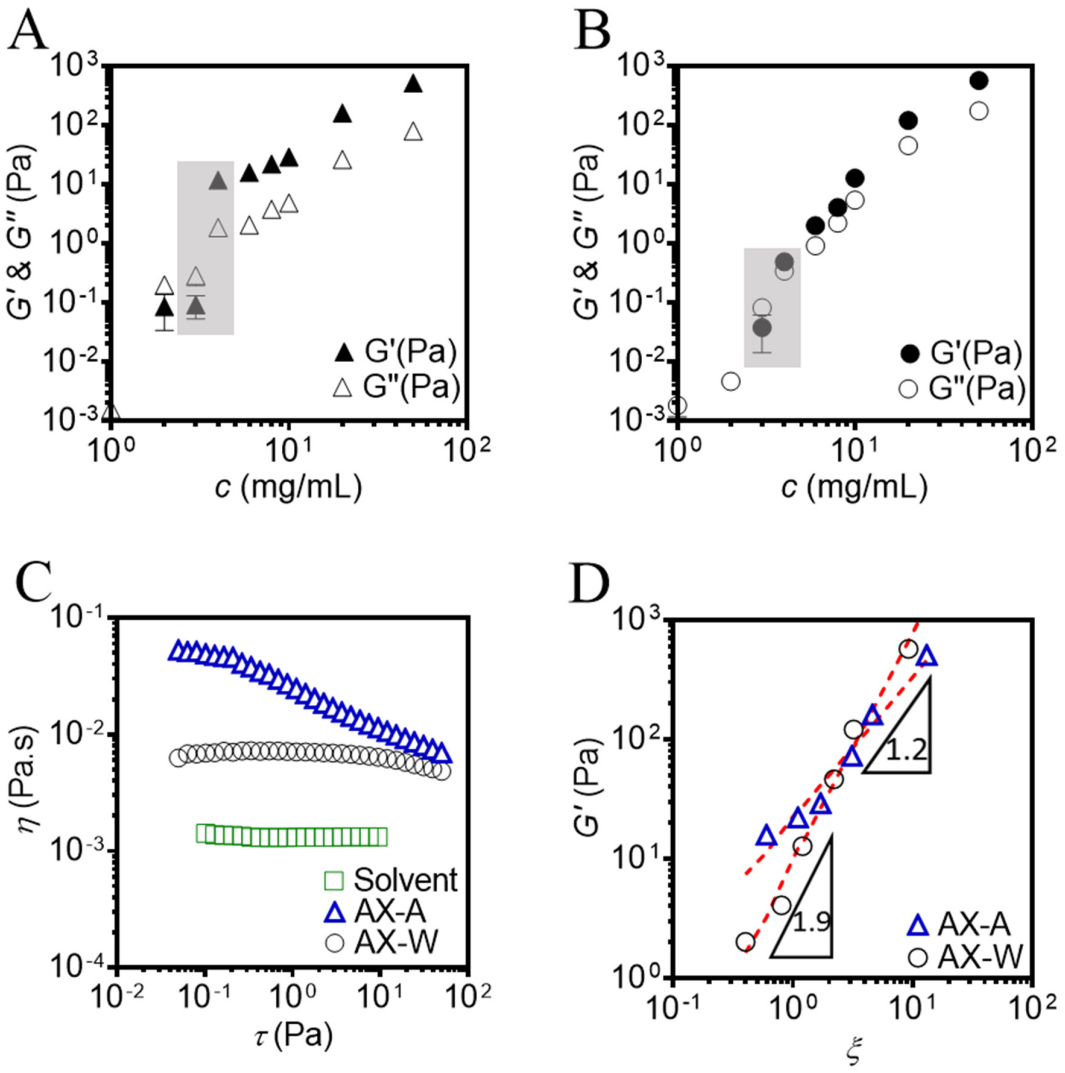

Figure. 1 Moduli for AX-A fraction (**A**) and AX-W fraction (**B**) as a function of increasing concentration in water; The shaded areas indicate the sol-gel transition region. (**C**) A steady shear test of 0.5% (w/v) AX fractions in 8 M GuHCl at 25°C. The influence of other chaotropic solvents on rheological behaviour of AX fractions is shown in supplementary Figure S1. (**D**) The plot of *G'* against ξ above the sol-gel transition point in water; $\xi = (c-c_g)/c_g$ where c is sample concentration, and c_g is the gelling concentration. The dash lines are power law model fits.

149

150 It has to be noted that the observed sol-gel transition (shaded area in Figures 1A and 1B) occurs
151 within the same range of concentration, despite a marked difference in absolute values of *G'*
152 and *G"*. Previously, we have demonstrated that the transition from the semi-dilute to entangled
153 solutions (c_e*) in "good" solvent (0.2 M KOH_{aq}) occurs for both fractions at identical values
154 of volume concentration, $c_e^*[\eta] = 4$ mL/mL, which corresponds to $c_e^* \approx 5.4$ mg/mL and ≈ 7.1
155 mg/mL for AX-A and AX-W fractions, respectively (Yu, Yakubov, Martínez-Sanz, Gilbert

and Stokes 2018). Surprisingly, the values of c_e* in 0.2M KOH are comparable with the gelling concentrations in pure water, $c_g \approx 4$ mg/mL, thereby suggesting that the onset of elasticity-dominated behaviour is likely to be associated with the entanglement transition, which in itself is determined by the molecular weight and persistence length of the polymer. The rationalisation of this result is that both fractions have similar molecular weight: 953 kDa and 971 kDa for AX-A and AX-W fractions, respectively (Yu, Yakubov, Zeng, Xing, Stenson, Bulone and Stokes 2017), as well as comparable values of the persistence length (Yu, Yakubov, Martínez-Sanz, Gilbert and Stokes 2018).

The differences between AX-A and AX-W fraction stem from the associative nature of these polymers, which was previously hypothesised to be due to the formation of intra-molecular hydrogen bonds (Yu, Yakubov, Gilbert, Sewell, van de Meene and Stokes 2019, Yu, Yakubov, Martínez-Sanz, Gilbert and Stokes 2018, Yu, Yakubov, Zeng, Xing, Stenson, Bulone and Stokes 2017) that are crucial for controlling 'gel-gel' adhesion and self-healing fusion of the material. The difference in the degree of hydrogen bonding has been postulated but never been characterised in detail. To address this knowledge gap, we, initially, perform an illustrative test by switching water to 8M GuHCl, the chaotropic solvent that markedly reduces the strength of hydrogen bonds. For this test, we have chosen the polymer concentration of 5 mg/mL, which sits just above the sol-gel transition. The results shown in Figure 1C demonstrate that both fractions lose the ability to form a gel in 8M GuHCl, confirming that hydrogen bonds are the key driver of gelation. Despite similarities, the AX-A fraction shows a markedly higher low-shear viscosity as well as a more pronounced shear thinning behaviour as compared to AX-W fraction. We note that both fractions have similar molecular weight and their molecular conformation was shown to be comparable based on the SANS scattering data (Yu, Yakubov, Gilbert, Sewell, van de Meene and Stokes 2019, Yu, Yakubov, Martínez-Sanz, Gilbert and Stokes 2018).

The key question to address is whether the AX-A fraction is characterised by the higher density of hydrogen bonds, or there is a qualitative difference in the strength of hydrogen bonds between AX-A and AX-W fractions. Under solvent conditions that suppress hydrogen bonds, the observed differences in rheological behaviour may favour the hypothesis that hydrogen bonds in AX-A fraction are stronger compared to AX-W fraction, and hence AX-A polymers may retain a certain degree of associative character even in 8M GuHCl. The residual hydrogen bonds can be sufficient to allow formation of AX-A supramolecular complexes that behave under shear as if they have higher molecular weight, giving rise to the pronounced shear

thinning behaviour. We note that at high shear stresses, the viscosity of both fractions converges, suggesting that upon shear and potential breakdown of supra-molecular aggregates the hydrodynamic volume of AX-A and AX-W polymers becomes similar (Pan *et al.* 2018). Furthermore, we also utilised other chaotropic solvents to examine the effect of residual hydrogen bonds on rheological behaviour of AX fractions as shown in supplementary Figure S1. In all cases, we observe similar behaviour in each solvent, whereby AX-A fraction displays a more pronounced shear shinning compared to AX-W fraction. The behaviour of fractions dissolved in [Emim][DEP] shows the largest degree of similarity between the polymer, which, we hypothesise, may be associated with the higher viscosity of pure ionic liquid and, consequently, larger values of applied shear stresses; or else, it could indicate that [Emim][DEP] solvent renders similar level of residual hydrogen in both polymers.

The nature of hydrogen bonding can be further probed by referring back to the sol-gel transition plots. From Figures 1A and 1B, the AX-A fraction shows a more abrupt increase in modulus during the sol-gel transition, as well as the ratio of G" and G' (also named as tan δ) for the AX-A gels is markedly lower compared to the AX-W gels. Above the c_g, the value of G' of AX-A fraction increases slower compared to AX-W fraction. To quantify this difference, the power law model is fitted to the data. At concentration near the sol-gel transition, the G' scales with the parameter $\xi = (c\text{-}c_g)/c_g$ as $G' \propto \xi^z$, where z is the power law exponent. The parameter ξ describes the measure of how far the concentration departs from the sol-gel transition or gelling point (c_g). Based on the Rouse model that assumes the hydrodynamic interaction is negligible(Martin *et al.* 1988), the value of z is predicted to be 2.7. The scalar elasticity percolation approximation (the nodes-links-blobs model) (Axelos and Kolb 1990, Martin and Adolf 1991) predicts the value of z to be 1.94. This power law effectively reflects the hydrodynamic interaction and geometric probability of forming an intermolecular cross-link with increasing the concentration of available binding sites.

As shown in Figure 1D, the AX-W fraction shows the scaling power of 1.9, which is consistent with the prediction of percolation theory. The power law exponent for AX-A is lower, $z = 1.2$, which suggests that the number of cross-links increases slower with concentration compared to the AX-W fraction, or else the cross-links formed in AX-A fraction are progressively weaker. To elaborate the latter hypothesis, we assume that AX-A polymers can form 'strong' and 'weak' intra-molecular hydrogen bonds. At low concentrations, the mobility of molecules is high which may favour the formation of 'strong' hydrogen bonds. The intuitive picture of such mechanism can be framed as follows: when system is dilute, each binding site can diffusively

'find' its 'strong' counterpart, which enables the system to find its thermodynamic (in terms of enthalpy) minimum. In concentrated and heavily entangled systems, on the other hand, the mobility is restricted which puts kinetic and thermodynamic constrains (entropy-driven) on possible molecular re-arrangements, leading to the scenario where not all 'strong' bonds can be allowed to form. The proposed mechanism can explain the abrupt change of modulus at the sol-gel transition in AX-A fraction, followed by the slow increase of *G'* with the subsequent increase of ξ.

If the similar concept is applied to explain viscoelastic behaviour of AX-W fraction, we propose AX-W polymers feature weaker and less specific interactions, so that regardless of the degree of entanglement (as indicated by the parameter ξ), hydrogen bonds still form with approximately same probability.

3.2 Difference in energy of hydrogen bonding

The differences in hydrogen bonding between AX-A and AX-W fractions can also be deduced from the distinct effect of temperature and pH on their viscoelastic properties. As shown in Supplementary Figure S2, the gel formed by AX-W fraction is more sensitive to the changes in temperature and pH compared to AX-A fraction. When temperature increases to 45 °C or pH reaches 12, the AX-W gel begins to behave like viscoelastic liquid ($tan\ \delta > 1$) rather than a gel-like fluid ($tan\ \delta < 1$). In contrast, AX-A fraction maintains its gel-like state from 25 to 65 °C as well as from pH 3 to 12.

To test the relative strength of hydrogen bonds in AX-A and AX-W fraction, we have utilised the hydrogen bond dynamics approach. Within this approach, the rate of dissociation of hydrogen bonds follows the transition state theory, whereby hydrogen bond lifetime ($\tau_H = 1/k_d$) is proportional to the activation free energy (ΔG^*) via the modified Arrhenius equation(Zheng and Fayer 2007):

$$\frac{1}{\tau_{\mathrm{H}}} = k_{\mathrm{d}} = \frac{k_{\mathrm{B}}T}{h} e^{-\Delta G^*/RT} = \frac{k_{\mathrm{B}}T}{h}\left(e^{\Delta S^*/R}\right)\left(e^{-\Delta H^*/RT}\right) \qquad (1)$$

T is temperature, R is the gas constant, ΔS^* is the activation entropy, ΔH^* is the activation enthalpy, k_B is the Boltzmann constant and h is the Plank constant.

In order to probe the activation energy for hydrogen bond dissociation, we have utilised the generic equation for elastic free energy (ΔU) (L. D. Landau *et al.* 2012), which for pure shear deformation is related to the shear stress and the strain (γ) in the form:

$$\Delta U = G\gamma^2 \quad (2)$$

where G is the complex shear modulus. Under experimental conditions of constant shear strain, the energy becomes simply proportional to the shear modulus. This simplification enables using the G' data as a measure of free elastic energy and thus enables applying the Arrhenius equation (1) to obtain the activation energy of hydrogen bond dissociation.

From the experimental perspective, we have chosen 8 mg/mL concentration, which is the highest concentration for which both fractions are found to undergo melting transition with increasing temperature. The concentration of 8 mg/mL is also relatively close to the sol-gel transition concentration; hence, the effects of entanglements and the restricted mobility of polymer chains – which can inhibit site-specific hydrogen bonds – are less dominating. As can be seen from Figure 2A, in vicinity of gel melting, the modulus dramatically decreases with the increase of temperature, which reflects the decrease in the extent of hydrogen bonding within the gel network. The activation energy (E_a) of the melting transition, therefore, provides the measure of the overall strength of hydrogen bonds that were broken during melting. The value of E_a is calculated based on Arrhenius equation (1):

$$log\ G' = A + \frac{E_a}{R}\ log\ (1/T) \quad (3)$$

where G', A, R and E_a are the storage modulus, pre-exponential factor, gas constant and activated energy, respectively. Figure 2B is the Arrhenius plot of both fractions near melting temperature with the slope corresponding to the value of $\frac{E_a}{R}$. The calculated values of E_a for AX-W fraction is 88.(6) kJ/mol, which is smaller than 101.(3) kJ/mol calculated for AX-A fraction. The higher value of E_a of AX-A fraction indicates the larger energy stored in hydrogen bonds that maintain its gel network.

In addition to the rheological methods, we have attempted to utilise DSC to measure the enthalpy of gel melting. The DSC thermograph show no obvious peaks between 25°C to 75°C (Supplementary Figure S3), which implies that the melting is a continuous process with potentially a broad energy distribution of hydrogen bonds whose dissociation is smeared across a relatively broad range of temperatures.

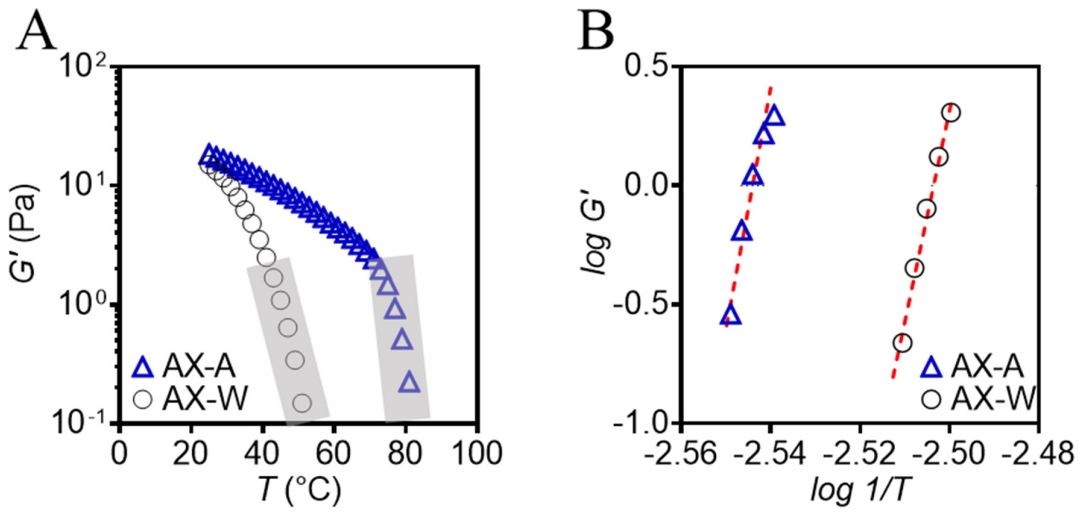

Figure 2. (**A**) *G'* as a function of temperature. The points inside the shaded area indicate the *G'* values used for Arrhenius plot as shown in panel B. (**B**) The Arrhenius plot of 0.8% (w/w) AX-A and AX-W fraction during gel melting process. The dash lines are the plots of Equation 3.

3.3 Evolution of gel network in non-linear viscoelastic region and gel damage

Although E_a is a useful parameter to characterise the network of hydrogen bonds in the gel, it lacks specificity; E_a does depend on the number of hydrogen bonds per unit volume as well as the dissociation enthalpy of individual hydrogen bond. To explore the nature of hydrogen bonding further, we utilise large amplitude oscillatory shear (LAOS) rheological measurements. Figure 3 shows the dependency of modulus on strain for both fractions. Based on strain sweep data, the linear and non-linear viscoelastic regions can be clearly identified. At the small deformation, the materials response (*G'* & *G"*) is independent of the magnitude of the deformation as shown in the linear viscoelastic region of Figure 3A and B. At the large deformation, the materials response depends on the magnitude of the deformation due to the disruption of internal structure, which is the non-linear viscoelastic region. As expected for hydrogels, the value of *G'* is always higher than that of *G"* for both fractions in the linear viscoelastic region (Figure 3A and B). However, the value of *G'* and the difference between *G'* and *G"* for AX-A fraction is higher compared to AX-W fraction, which is consistent with the AX-A hydrogel being stronger than AX-W hydrogel. In the non-linear region, both fractions show 'weak-strain-overshot' feature with a pronounced local maximum in the *G"*, which has been observed in soft glassy materials and weak hydrogels (Hyun *et al.* 2011). The structural cause of the strain overshoot behaviour in *G"* is not clear, but one possible explanation is the increase of the effective volume of temporal network structures that undergo large deformation

295 (Tirtaatmadja *et al.* 1997). Compared to AX-A hydrogel, the AX-W hydrogel shows smooth
296 transition from the linear to non-linear viscoelastic region.

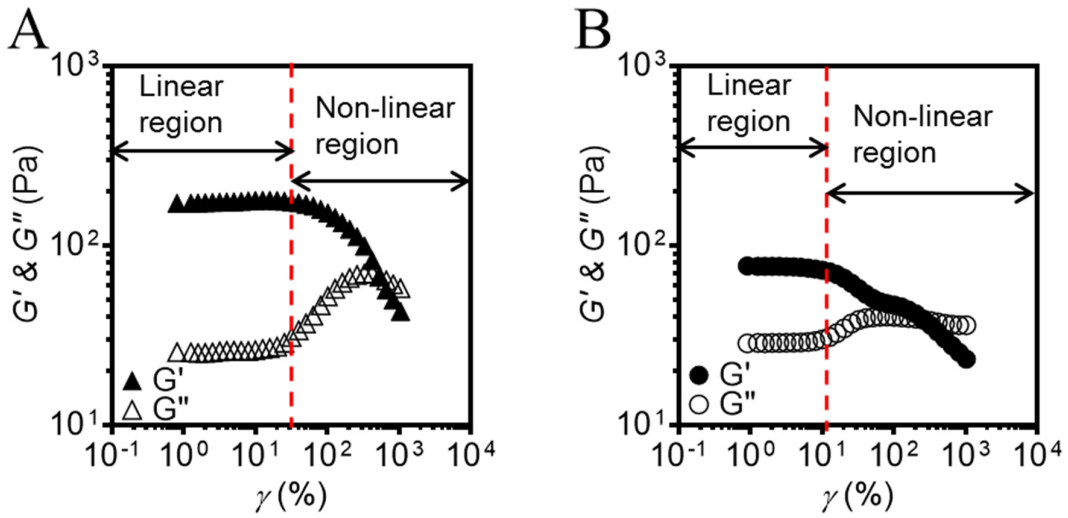

Figure 3. Strain sweep measurements of 2% (w/v) AX-A (**A**) and AX-W (**B**).

297 To characterise the non-linear viscoelastic behaviour of the material response to the imposed
298 sinusoidal oscillating strain, we have plotted LAOS data in a form of Lissajous plots. The total
299 response stress (σ) can be decomposed into an elastic part (σ') and a viscous part (σ''), which
300 are related to strain and strain-rate as shown in following equation (4) and (5):

$$\sigma' \equiv \frac{\sigma(\Upsilon,\dot{\Upsilon}) - \sigma(-\Upsilon,\dot{\Upsilon})}{2} \tag{4}$$

$$\sigma'' \equiv \frac{\sigma(\Upsilon,\dot{\Upsilon}) - \sigma(\Upsilon,-\dot{\Upsilon})}{2} \tag{5}$$

301 The Lissajous curves of total stress response against strain provide an 'elastic perspective' of
302 the three dimension space curve $\sigma(\Upsilon,\dot{\Upsilon})$, while the Lissajous curves of total stress response
303 against strain rate provide a 'viscous perspective' (Cho *et al.* 2005). As shown in Figure 4, a
304 selection of strain amplitudes from oscillatory strain sweep are performed on AX-A and AX-
305 W fractions at 6.28 rad/s and 25°C. In 'elastic' Lissajous curves (Figure 4A and C), both
306 fractions show elliptical shape at small deformation. However, with increasing strain, the
307 elliptical shape curves become banana-like shape for AX-A fraction but rectangle for AX-W
308 fraction. Moreover, in 'viscous' Lissajous curves (Figure 4B and D), both fractions show
309 similar elliptical shape under small deformation, but they become distinctively different under
310 large deformation.

311 The geometrically-defined dynamic moduli (G'_M & G'_L) and dynamic viscosity (η'_M and η'_L)
312 can be obtained from 'elastic' and 'viscous' Lissajous curves respectively (Ewoldt *et al.* 2008),
313 which quantify the non-linear behaviour of the material and characterise the evolution of
314 hydrogel network damage. As shown in Figure 5A, the dashed line represents the dynamic
315 tangent modulus G'_L at conditions corresponding to maximum strain ($\Upsilon = \Upsilon_0$) and zero strain
316 rate ($\dot{\Upsilon} = 0$), while the dot dashed line represents the dynamic elastic tangent moduli G'_M at
317 minimum strain ($\Upsilon = 0$) and maximum strain rate ($\dot{\Upsilon}_0 = \omega\Upsilon_0$). The G'_M represent the onset of
318 plastic flow in the material and G'_L reveals the accumulation of damage within the elastic
319 network. We thus use these two parameters to quantify the solid-fluid transition of soft
320 hydrogels under dynamic loading based on following equation (6) (Faber *et al.* 2017):

$$\phi \equiv \frac{G'_L - G'_M}{G'_L} \tag{6}$$

321 ϕ is a fluidizing ratio, which is a measure of the extent to which the elastic solid gel has
322 transitioned into a flowing fluid.

323

324

325

326

327

328

329

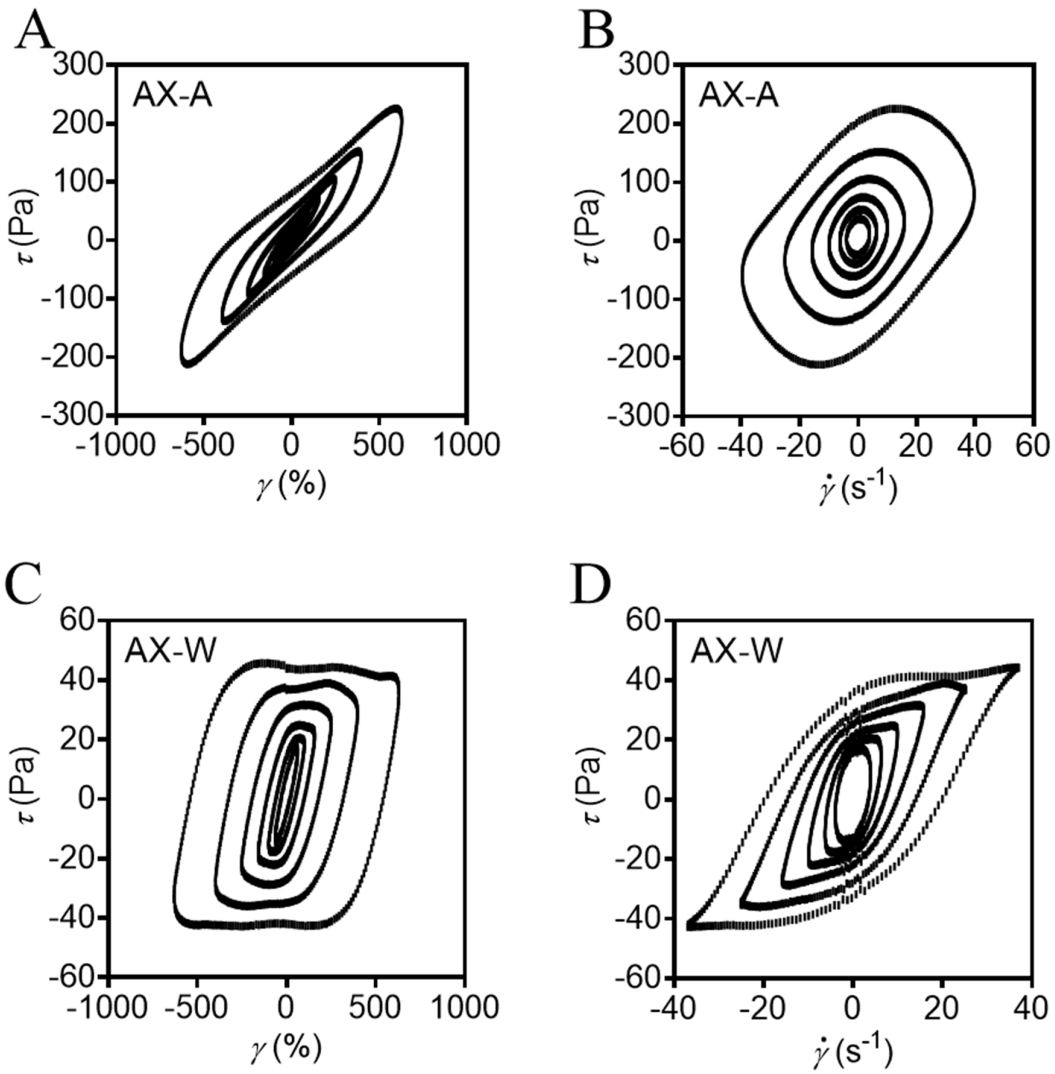

Figure 4. The solid-fluid transition of AX-A and AX-W fractions at T = 25 °C and ω = 6.28 rad/s depicted using the Lissajous curves of total stress response against strain (**A,C**) or strain rate (**B,D**) at different initial strain amplitudes from 63% to 630%.

330

331

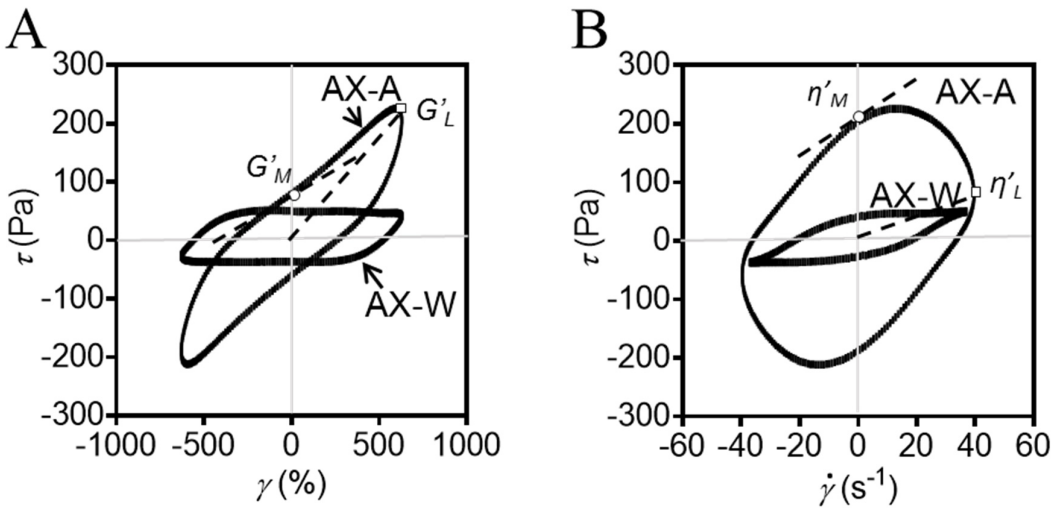

Figure 5 The Lissajous curves of total stress response plotted against strain (**A**) or strain rate (**B**) at strain amplitudes of 630% for AX-W and AX-A fraction. The hollow circle (❍) and square (❑) markers show the intra-cycle maxima and minima of the viscous stress, respectively. In Panel **A**, the dashed line through the point marked by the hollow circle is the tangent modulus at maximum strain rate, G'_M, and the dashed line through the point marked by the hollow square is the secant modulus at maximum strain, G'_L. In Panel **B**, the dashed line through the point marked by the hollow circle is the minimum-rate dynamic viscosity, η'_M, and the dashed line through the point marked by the hollow square is maximum-rate dynamic viscosity, η'_L.

Figure 6A shows the fluidizing ratio plotted against shear strain. At the low strain region, the fluidizing ratio of both fractions is close to zero, which reveals that there is no plastic flow. When strain is above 100%, the value of ϕ of both fractions dramatically increases, suggesting microcracks nucleate and propagate in the gel matrix and induce fluidisation. With the further increase of strain, the value of ϕ of AX-W fraction continues increasing but that of AX-A fraction remains constant with a small upturn at 630% strain. These results indicate that AX-A hydrogel is more resilient to large strain with less significant gel matrix damage compared to AX-W hydrogel.

By analogy to the definition of fluidisation, the dynamic tangent viscosity η'_L at maximum strain rate and η'_M at zero strain rate are obtained from Figure 5B. The thickening ratio (Θ) is defined as the evolution of the solid-fluid transition from the viscous perspective (Equation 7) (Faber, Van Breemen and McKinley 2017):

$$\Theta \equiv \frac{\eta'_L - \eta'_M}{\eta'_L} \tag{7}$$

From the viscous perspective, Figure 6B reveals a different pattern of solid-fluid transition under large deformation for AX-A and AX-W hydrogels, respectively. The value of Θ of AX-

A fraction is negative and decreases with an increase of strain rate, suggesting 'shear-thinning'-like behaviour. In contrast, the value of Θ of AX-W fraction is always positive, revealing 'shear-thickening'-like behaviour.

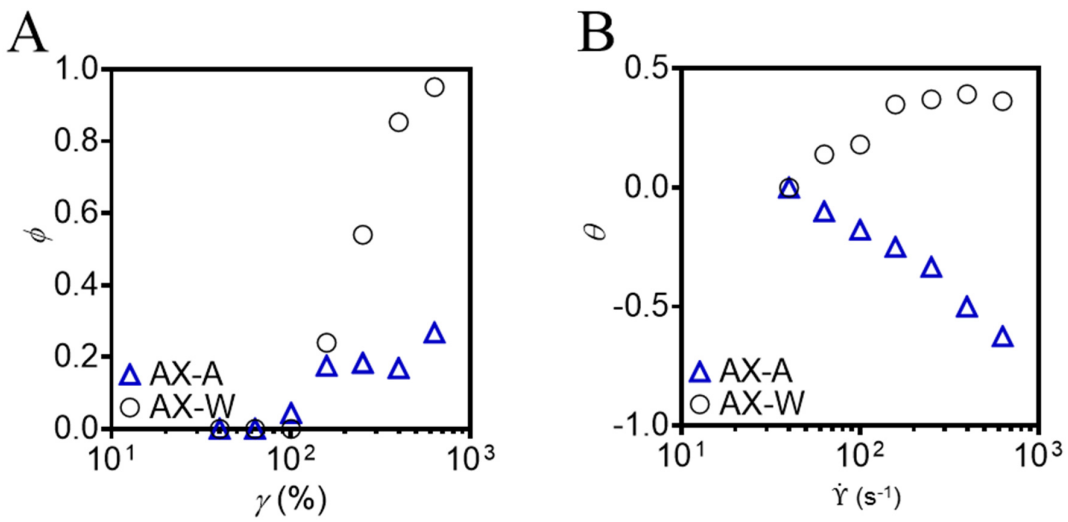

Figure 6 Strain sweeps showing the evolution in (**A**) the fluidizing ratio, and (**B**) the thickening ratio of AX-W and AX-A fractions at 25 °C and ω = 6.28 rad/s.

To rationalize the results showing the gel network damage in non-linear viscoelastic region, we consider the gel architectures of AX-A and AX-W fractions. The Cyro-SEM microscopy images shown in Figure 7 show a similar porous network structure. Based on our previous studies, we identify that the networks of both AX-A and AX-W hydrogels are stabilised by hydrogen bonding between the side-chains. Therefore, different behaviours of these hydrogels under large deformation may depend on the distinct strength and/or distribution of hydrogen bonding within the gel matrix. The AX-W gel network is more "viscous" and breaks less 'abruptly' upon increasing strain compared to the AX-A gels, which may indicate that the strength of the hydrogen bonding between AX-W side chains is weaker than for the AX-A fraction. The observed 'shear thickening'-like behaviour suggests that 'weak' hydrogen bonds in AX-W reform very quickly after being broken by the applied deformation, thus restoring molecular associations. In contrast, the AX-A fraction may contain both 'weak' and 'strong' hydrogen bonds; while the 'strong' hydrogen bonds provide high resilience against large deformations, from the 'viscous perspective', AX-A gels show 'shear-thinning' behaviour because the 'weak' hydrogen bonds in AX-A may be less numerous and hence insufficient to support large scale molecular associations.

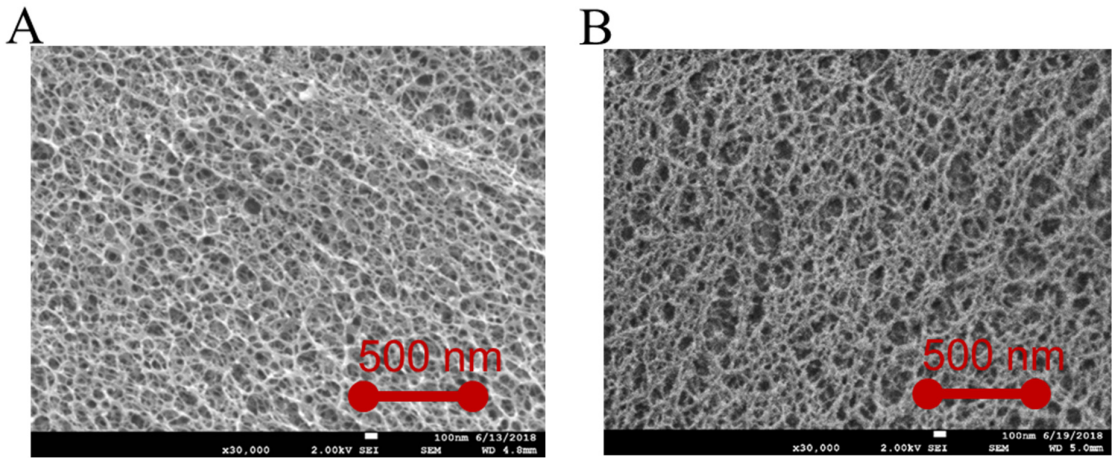

Figure 7. Cyro-SEM SEM images of 5% AX-A (**A**) and AX-W (**B**) hydrogels taken at 30,000 magnification. The scale bar is 0.5 µm.

3.4 Rapid and slow self-healing property

Based on the analyses of gel behaviour under LAOS, we propose that a more rapid formation of "weak" hydrogen bonds leads to a faster rate of self-healing properties in AX-W fraction. To probe the recovery of the gel network after disruption under conditions of applied shear strain, the oscillatory amplitude step tests were utilised. As shown in Figures 8A and 8B, the tests started at the applied oscillatory amplitude of 5%, which corresponds to the linear viscoelastic regime. Then, in a stepping manner, the amplitude was increased to 1000% and 500% for AX-A and AX-W fraction, respectively. As shown in Figures 8A and 8B, the G' decreases and becomes lower than G" after application of the large strain. By applying the high strain, the gels were transitioned into a shear-induced molten state characterised by $\tan\delta \approx 0.75$. Once the strain reverts back to 5%, G' recovers at a certain rate, which provides a quantitative measure of the autonomous self-healing process. The stepping tests were repeated twice, and the G' recovery curve was modelled using an empirical two-mode relaxation model:

$$G' = G'_0 + (G'_{max} - G'_0) \cdot \left[\alpha\left(1 - e^{-\frac{t-t_0}{\tau_1}}\right) + (1-\alpha)\left(1 - e^{-\frac{t-t_0}{\tau_2}}\right)\right] \quad (8)$$

G'_0 is the initial value of G', G'_{max} is the asymptotic 'recovered' value of G', α is the relaxation factor, $(t - t_0)$ is the offset time, and τ is the relaxation time. The fitting parameters are summarised in Supplementary Table 1.

Based on the analysis using eq 8, the recovery behaviour of AX-A gels can be described using a model with two relaxation modes: 'fast' and 'slow'. The proportion of the 'fast' mode is found to be 40% (parameter $\alpha = 0.4$) with characteristic relaxation time of the order of tens of

seconds. The 'slow' relaxation mode, which dominates the recovery process (parameter α' = (1 - α) = 0.6) was found to have characteristic relaxation time of the order of a few minutes. We note that the second gel disruption-recovery cycle is characterised by longer relaxation times. The increase of relaxation time is likely to be associated with incomplete recovery of the gel during the low strain amplitude step. The corroborated recovery behaviour is consistent with the hypothesis of 'weak' and 'strong' hydrogen bonds, which recover 'fast' and 'slow', respectively.

The recovery behaviour of AX-W gels is described by a single exponential mode (parameter α = 1), with the values of relaxation time being found in the range between 20 and 30 s. These values are very close to the relaxation time attributed to the 'fast' relaxation mode found in the AX-A gels. We also note that due to short relaxation time of gel recovery of AX-W gels, *G'* fully recovers during the low strain amplitude step. Consequently, the values of characteristic relaxation time remain roughly unchanged between the first and the second recovery steps (i.e., 22.3 ± 1.0 versus 25.7 ± 7.4 s, respectively). The corroborated recovery behaviour is consistent with the hypothesis that AX-W is dominated by 'fast'-dissociating ('weak') hydrogen bonds, whilst the contribution from the 'slow'-dissociating bonds is negligible.

Using the analysis above, it is possible to estimate the lower bound for the energy of the 'strong' hydrogen bonds. From the Arrhenius analysis of temperature induced melting (Section 3.2), we conclude that 'weak' hydrogen bonds, which dominate the recovery response of AX-W gel, average ~ 90 kJ/mol. At the same time, the combination of 'weak' and 'strong' bonds found in AX-A gels results in the average of ~101 kJ/mol. Using the values of parameter α from eq. 8, we estimate the energy of 'strong' hydrogen bonds as: $\left(101\,\frac{\mathrm{kJ}}{\mathrm{mol}} - \alpha \cdot 90\,\frac{\mathrm{kJ}}{\mathrm{mol}}\right)/(1-\alpha)$. Plugging the value of α = 0.4, the lower bound of the average energy of 'strong' bonds is estimated to be ~110 kJ/mol, which is comparable with the bond enthalpy between guanine and cytosine in DNA.

The self-healing behaviour of AX-A and AX-W hydrogels can also be illustrated using a very simple demonstration of differences in the rate of interfacial fusion between pairs of hydrogels. In this demonstration, we have prepared two hydrogel blocks (Figure 8C-I and 8D-I) and put them together (Figure 8C-II and 8D-II). Then, the top hydrogel block is pulled up by a tweezer in order to separate from the bottom hydrogel block. We find that two AX-W hydrogels fuse together rapidly (~ 20 s) upon contact, and the top and the bottom hydrogel blocks are pulled up together (Figure 8D-III). In contrast, the self-healing process of two AX-A hydrogels is

much slower so the top hydrogel block is separated from the bottom one (Figure 8C-III). After a prolonged period of time (4 h), both AX-A and AX-W fractions fuse together with the boundary between green and white hydrogels vanishing, resulting in the formation of a single cylinder-like green block of hydrogel (Figure 8C-IV and 8D-IV, for AX-A and AX-W hydrogels, respectively).

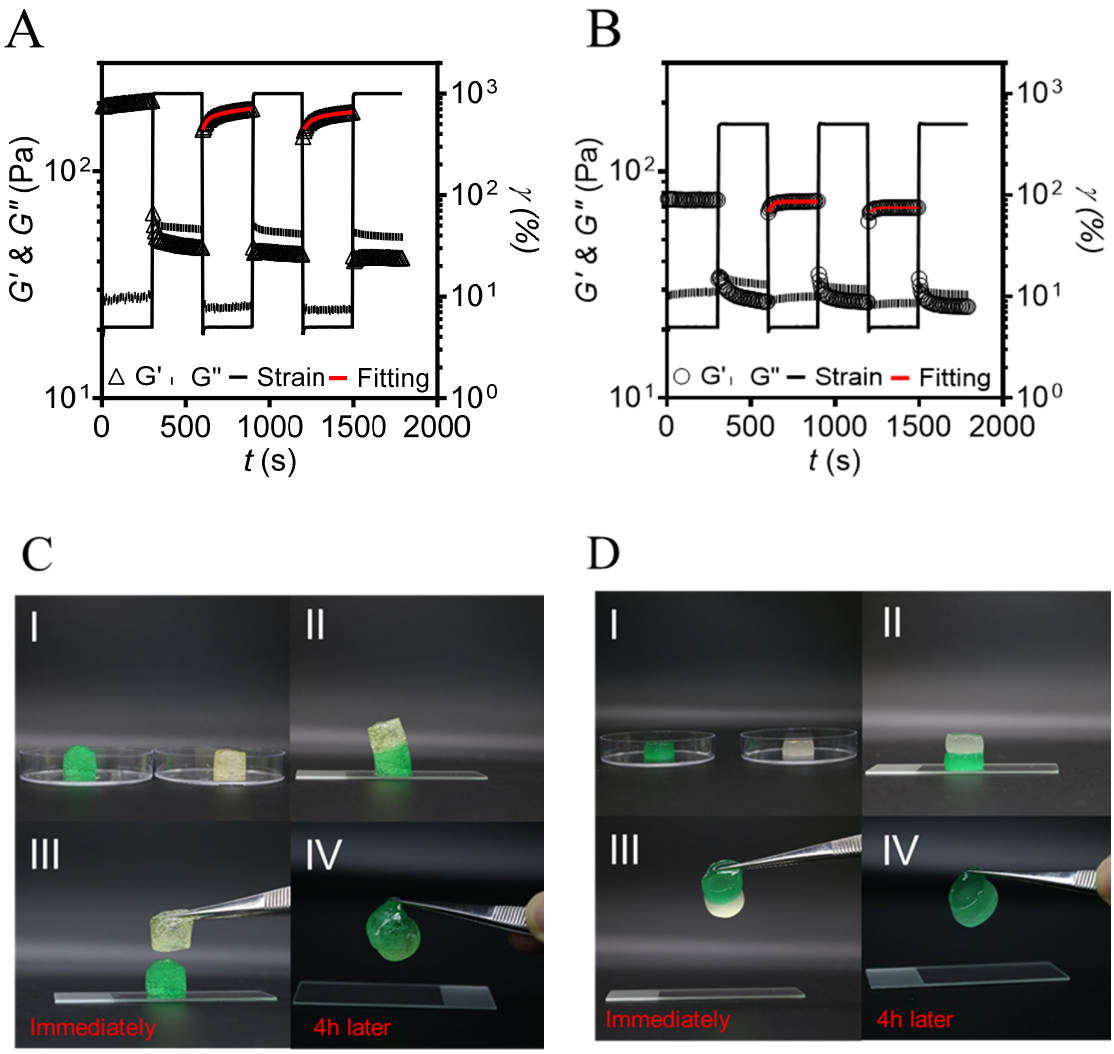

Figure 8. (**A**, **B**) Cyclic strain-recovery test performed using 5% (*w/v*) AX-A fraction (**A**) and AX-W fraction (**B**). Lines show the model fits using eq 8. The fitting parameters are summarised in Supplementary Table 1. (**C**, **D**) Dynamic interfacial fusion demonstration using pairs of AX-A (**C**) and AX-W hydrogels (**D**).

4. Conclusion

We have established the link between the properties of intermolecular hydrogen bonds and rheological and micromechanical properties of hydrogels formed by complex brush-like arabinoxylans extracted from *Plantago ovata* seed mucilage. In particular, we focus on two polysaccharide fractions with similar molecular weight distribution, linkage composition and gels microstructure, which – contrary to expectation – are characterised by a distinct set of rheological properties(Yu, Yakubov, Zeng, Xing, Stenson, Bulone and Stokes 2017). Here we show that differences in the rheological properties stem from the distinct distribution of the strengths of hydrogen bonds between polymer side chains. For the thermos-sensitive gels formed by hot water extractable AX fraction (AX-W), these hydrogen bonds are characterised as comparatively 'weak' ('fast'-dissociating) with a molar energy of 90 kJ/mol. In contrast, the thermo-stable AX-A gels are characterised by the presence of 'weak' and 'strong' hydrogen bonds, with the latter 'slow'-dissociating and having an estimated molar energy of 110 kJ/mol. The presence of different types of hydrogen bonds affects the linear and non-linear viscoelastic behaviour of hydrogels: the weak hydrogen bonds contribute to viscous gel properties but fast self-healing behaviour, while the strong hydrogen bonds lead to elastic gel properties but slow self-healing behaviour. The balance between the weak and strong hydrogen bonding determines the rate of gel structure recovery, which is associated with autonomous self-healing rate of these hydrogels.

It is hypothesised that the difference between different AX fractions stems from the differences in the distribution (motif) of side chains, which previously was observed in plant cell wall heteroxylans (Berglund *et al.* 2016, Grantham *et al.* 2017, Martinez-Abad *et al.* 2017, Simmons *et al.* 2016). Therefore, it is possible to manipulate the strength and distribution of hydrogen bonds within the gel matrix through control over the motif of side chain distribution of polysaccharide. This research opens new possibilities of rational design of natural hydrogels with programmable rheological and self-healing properties. We also note that structural similarity of AX-A and AX-W gels reported by us previously (Yu, Yakubov, Gilbert, Sewell, van de Meene and Stokes 2019) are likely to stem from the static nature of scattering experiments, which precluded from probing the dynamic (dissociative) nature of hydrogen bonds. It becomes apparent that rheological techniques provide a markedly more sensitive tool to probe intermolecular interactions in polysaccharide physical gels and open new opportunities and avenues for characterising and resolving dynamic structures formed by complex carbohydrates.

5. Acknowledgements

The authors thank Dr Matthew Tucker and Prof Rachel Burton (University of Adelaide) for providing *P.ovata* seeds. Dr Kim Sewel is acknowledged for SEM imaging of hydrogels. L.Y. acknowledges financial support of the UQ International Postgraduate Research Scholarship. J.R.S. and G.E.Y. acknowledge financial support of the Australian Research Council Discovery Project (DP150104147). The research is supported by an Australian Research Council Centre of Excellence in Plant Cell Walls (CE110001007).

6. References

Axelos, M., and Kolb, M., ‘‘Crosslinked biopolymers: Experimental evidence for scalar percolation theory,’’ Physical review letters 64, 1457 (1990).

Berglund, J., d'Ortoli, T. A., Vilaplana, F., Widmalm, G., Bergenstrahle-Wohlert, M., Lawoko, M., Henriksson, G., Lindstrom, M., and Wohlert, J., ‘‘A molecular dynamics study of the effect of glycosidic linkage type in the hemicellulose backbone on the molecular chain flexibility,’’ Plant Journal 88, 56-70 (2016).

Blaiszik, B. J., Kramer, S. L., Olugebefola, S. C., Moore, J. S., Sottos, N. R., and White, S. R., ‘‘Self-healing polymers and composites,’’ Annual review of materials research 40, 179-211 (2010).

Cho, K. S., Hyun, K., Ahn, K. H., and Lee, S. J., ‘‘A geometrical interpretation of large amplitude oscillatory shear response,’’ Journal of rheology 49, 747-758 (2005).

Cui, J., and del Campo, A., ‘‘Multivalent H-bonds for self-healing hydrogels,’’ Chemical Communications 48, 9302-9304 (2012).

Ewoldt, R. H., Hosoi, A., and McKinley, G. H., ‘‘New measures for characterizing nonlinear viscoelasticity in large amplitude oscillatory shear,’’ Journal of Rheology 52, 1427-1458 (2008).

Faber, T., Van Breemen, L., and McKinley, G., ‘‘From firm to fluid–Structure-texture relations of filled gels probed under Large Amplitude Oscillatory Shear,’’ Journal of Food Engineering 210, 1-18 (2017).

Fischer, M. H., Yu, N. X., Gray, G. R., Ralph, J., Anderson, L., and Marlett, J. A., ‘‘The gel-forming polysaccharide of psyllium husk (Plantago ovata Forsk),’’ Carbohydrate Research 339, 2009-2017 (2004).

Grantham, N. J., Wurman-Rodrich, J., Terrett, O. M., Lyczakowski, J. J., Stott, K., Iuga, D., Simmons, T. J., Durand-Tardif, M., Brown, S. P., Dupree, R., Busse-Wicher, M., and Dupree, P., ‘‘An even pattern of xylan substitution is critical for interaction with cellulose in plant cell walls,’’ Nature Plants 3, 859-865 (2017).

Guimard, N. K., Oehlenschlaeger, K. K., Zhou, J., Hilf, S., Schmidt, F. G., and Barner‐Kowollik, C., ‘‘Current trends in the field of self‐healing materials,’’ Macromolecular Chemistry and Physics 213, 131-143 (2012).

Guo, Q., Cui, S. W., Wang, Q., and Young, J. C., ‘‘Fractionation and physicochemical characterization of psyllium gum,’’ Carbohydrate Polymers 73, 35-43 (2008).

Hoare, T. R., and Kohane, D. S., ‘‘Hydrogels in drug delivery: Progress and challenges,’’ Polymer 49, 1993-2007 (2008).

Hyun, K., Wilhelm, M., Klein, C. O., Cho, K. S., Nam, J. G., Ahn, K. H., Lee, S. J., Ewoldt, R. H., and McKinley, G. H., ‘‘A review of nonlinear oscillatory shear tests: Analysis and application of large amplitude oscillatory shear (LAOS),’’ Progress in Polymer Science 36, 1697-1753 (2011).

L. D. Landau, L. P. Pitaevskii, A. M. Kosevich, and Lifshitz, E. M., *Theory of Elasticity*, 3rd Edition ed. (Elservier, 2012).

Lee, K. Y., and Mooney, D. J., ‘‘Hydrogels for tissue engineering,’’ Chemical reviews 101, 1869-1880 (2001).

Martin, J., and Adolf, D., ‘‘The sol-gel transition in chemical gels,’’ Annual review of physical chemistry 42, 311-339 (1991).

Martin, J. E., Adolf, D., and Wilcoxon, J. P., ‘‘Viscoelasticity of near-critical gels,’’ Physical review letters 61, 2620 (1988).
Martinez-Abad, A., Berglund, J., Toriz, G., Gatenholm, P., Henriksson, G., Lindstrom, M., Wohlert, J., and Vilaplana, F., ‘‘Regular Motifs in Xylan Modulate Molecular Flexibility and Interactions with Cellulose Surfaces,’’ Plant Physiology 175, 1579-1592 (2017).
Pan, S., Nguyen, D. A., Dunweg, B., Sunthar, P., Sridhar, T., and Prakash, J. R., ‘‘Shear thinning in dilute and semidilute solutions of polystyrene and DNA,’’ Journal of Rheology 62, 845-867 (2018).
Richter, A., Paschew, G., Klatt, S., Lienig, J., Arndt, K.-F., and Adler, H.-J., ‘‘Review on hydrogel-based pH sensors and microsensors,’’ Sensors 8, 561-581 (2008).
Shewan, H. M., and Stokes, J. R., ‘‘Review of techniques to manufacture micro-hydrogel particles for the food industry and their applications,’’ Journal of Food Engineering 119, 781-792 (2013).
Simmons, T. J., Mortimer, J. C., Bernardinelli, O. D., Poppler, A. C., Brown, S. P., Deazevedo, E. R., Dupree, R., and Dupree, P., ‘‘Folding of xylan onto cellulose fibrils in plant cell walls revealed by solid-state NMR,’’ Nature Communications 7 (2016).
Taylor, D. L., and in het Panhuis, M., ‘‘Self‐healing hydrogels,’’ Advanced Materials 28, 9060-9093 (2016).
Tirtaatmadja, V., Tam, K., and Jenkins, R., ‘‘Superposition of oscillations on steady shear flow as a technique for investigating the structure of associative polymers,’’ Macromolecules 30, 1426-1433 (1997).
Yu, L., Yakubov, G. E., Gilbert, E. P., Sewell, K., van de Meene, A. M., and Stokes, J. R., ‘‘Multi-scale assembly of hydrogels formed by highly branched arabinoxylans from Plantago ovata seed mucilage studied by USANS/SANS and rheology,’’ Carbohydrate polymers 207, 333-342 (2019).
Yu, L., Yakubov, G. E., Martínez-Sanz, M., Gilbert, E. P., and Stokes, J. R., ‘‘Rheological and structural properties of complex arabinoxylans from Plantago ovata seed mucilage under non-gelled conditions,’’ Carbohydrate Polymers 193, 179-188 (2018).
Yu, L., Yakubov, G. E., Zeng, W., Xing, X., Stenson, J., Bulone, V., and Stokes, J. R., ‘‘Multi-layer mucilage of Plantago ovata seeds: Rheological differences arise from variations in arabinoxylan side chains,’’ Carbohydrate Polymers 165, 132-141 (2017).
Zheng, J., and Fayer, M. D., ‘‘Hydrogen bond lifetimes and energetics for solute/solvent complexes studied with 2D-IR vibrational echo spectroscopy,’’ Journal of the American Chemical Society 129, 4328-4335 (2007).
Zheng, W. J., An, N., Yang, J. H., Zhou, J., and Chen, Y. M., ‘‘Tough Al-alginate/poly (N-isopropylacrylamide) hydrogel with tunable LCST for soft robotics,’’ ACS applied materials & interfaces 7, 1758-1764 (2015).

Supplementary Figures

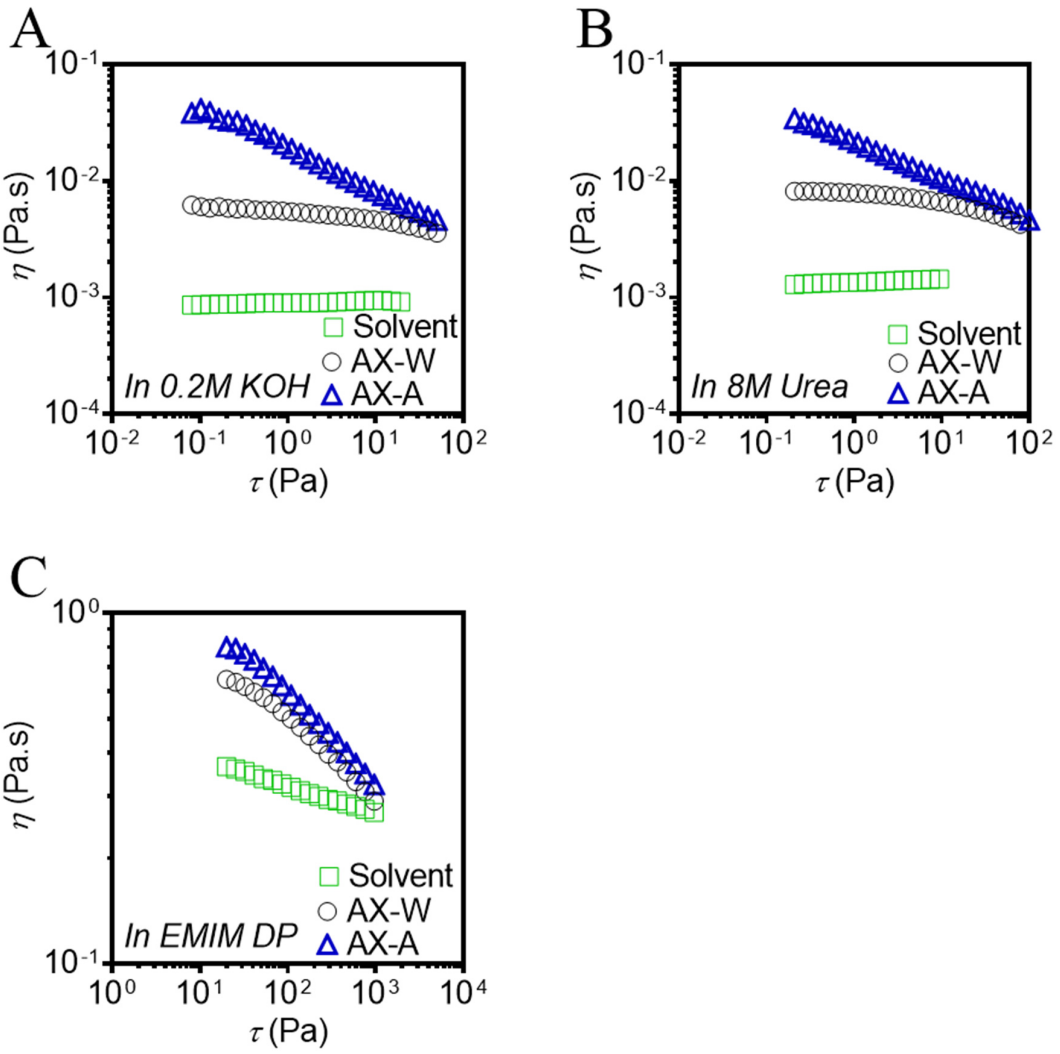

Supplementary Figure S1. Steady shear test of 0.5% (w/w) AX-A fraction and AX-W fraction in 0.2M KOH (**A**), 8M urea (**B**) and ionic liquid (**C**) at 25°C.

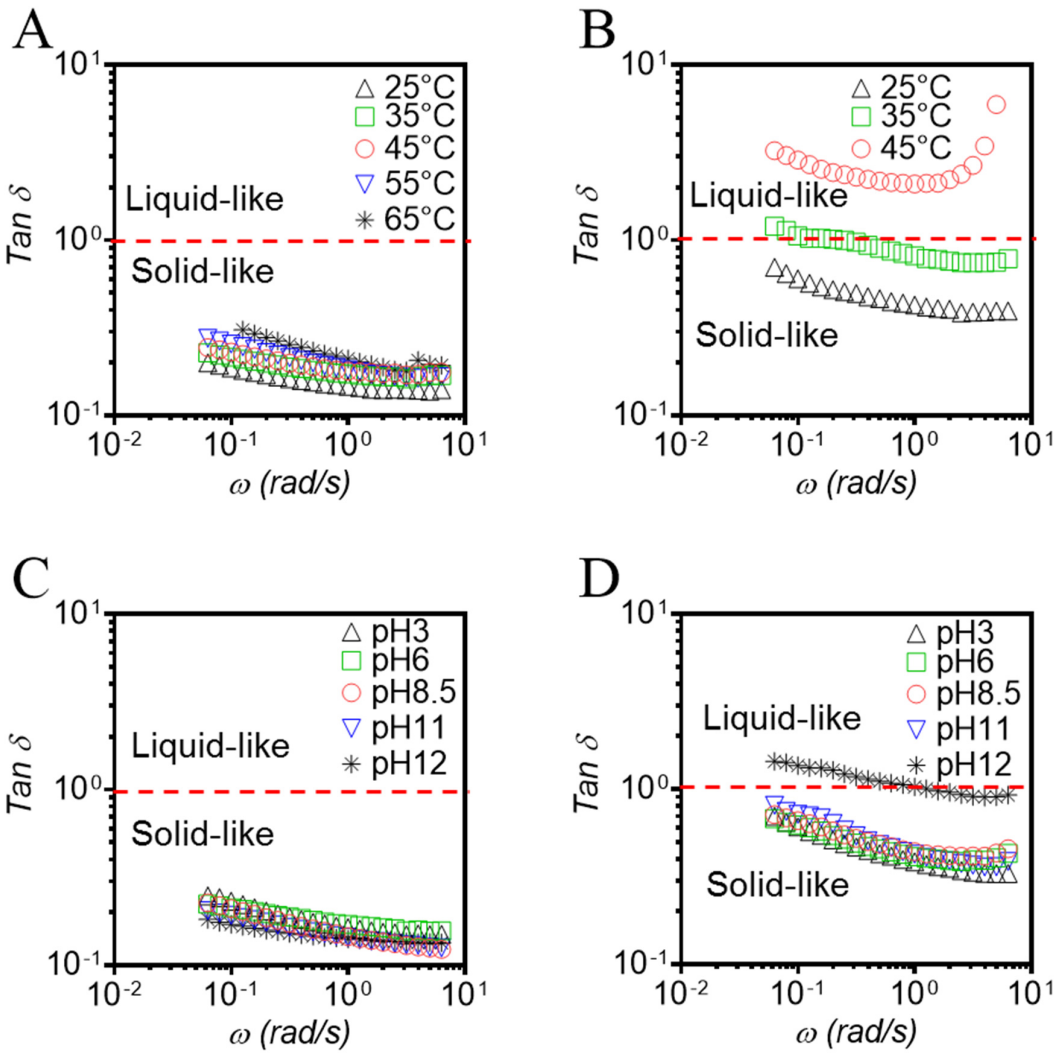

Supplementary Figure S2. The effect of pH and temperature on gelation of AX-A fraction (**A, C**) and AX-W fraction (**B, D**) at concentration of 0.8% (*w/v*).

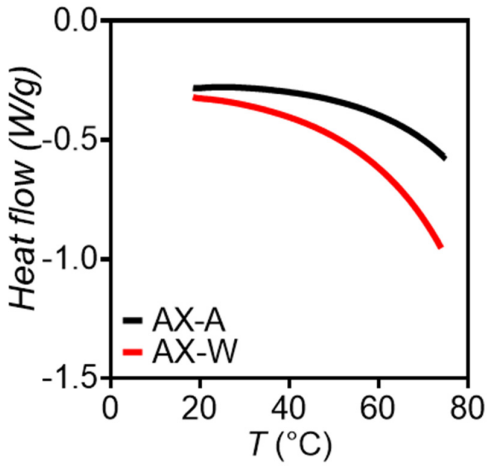

Supplementary Figure S3. DSC curves from 5% (*w/v*) AX-W and AX-A fraction during heating from 25 to 75 °C at a ramp rate of 3°C/min.

Supplementary Table

Supplementary Table 1. The fitting parameters of the dynamic gel recovery tests

	AX-A recover I	AX-A recover II	AX-W recover I	AX-W recover II
G'_0 [Pa]	150 ± 5	150 ± 5	65 ± 2	65 ± 3
G'_{max} [Pa]	200 ± 10	200 ± 10	73.6 ± 2.2	69.2 ± 0.6
α	0.40 ± 0.02	0.40 ± 0.02	1.00	1.00
t_1 [s]	23 ± 0.5	41 ± 1.5	22 ± 1	26 ± 7.5
t_2 [s]	297 ± 4	546 ± 10	---*	---

* For AX-W fraction single relaxation time model is applied ($\alpha = 1$).